Journal of Hazardous Materials 440 (2022) 129730

Contents lists available at ScienceDirect

Journal of Hazardous Materials

journal homepage: www.elsevier.com/locate/jhazmat

Research Paper

Water-fueled autocatalytic bactericidal pathway based on e-Fenton-like reactions triggered by galvanic corrosion and extracellular electron transfer

Jizheng Yao [a], Tao Jiang [a], Yucheng Ji [b], Biwen Annie An [c], Andrea Koerdt [c], Zhongqi Cai [a], Chaofang Dong [b], Yan Ge [a,*], Zhenhui Qi [a,*]

[a] Sino-German Joint Research Lab for Space Biomaterials and Translational Technology, Synergetic Innovation Center of Biological Optoelectronics and Healthcare Engineering (BOHE) Shaanxi Provincial Synergistic Innovation Center for Flexible Electronics & Health Sciences (FEHS), School of Life Sciences, Northwestern Polytechnical University, Xi'an, Shaanxi 710072, PR China

[b] Beijing Advanced Innovation Center for Materials Genome Engineering, Key Laboratory for Corrosion and Protection (MOE), Institute for Advanced Materials and Technology, University of Science and Technology Beijing, Beijing 100083, PR China

[c] Bundesanstalt für Materialforschung und -prüfung (BAM), Unter den Eichen 87, 12205, Berlin, Germany

HIGHLIGHTS

- Non-chemical and water-consuming disinfection strategy for combating microbial contamination in fuel system condition.
- Water-fueled autocatalytic (WFA) bactericidal pathway for spontaneously produce H_2O_2 and reactive oxygen species (ROS).
- Extracellular Electron Transfer (EET) and micro-galvanic corrosion provides the electron source for ORR.

GRAPHICAL ABSTRACT

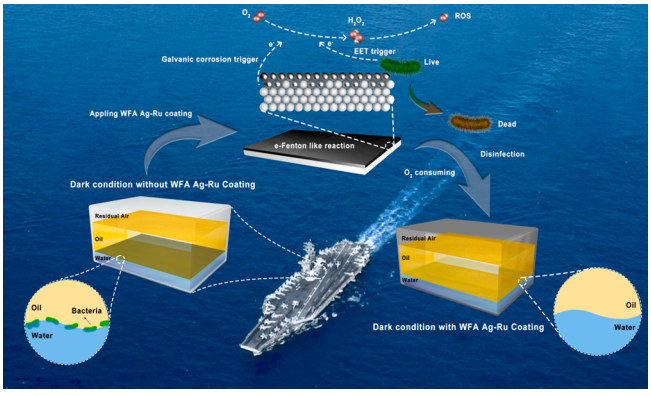

ARTICLE INFO

Editor: Danmeng Shuai

Keywords:
Fenton-like reaction
Reactive oxygen species
Disinfection
Fuel
Silver
Ruthenium

ABSTRACT

Water is generally considered to be an undesirable substance in fuel system, which may lead to microbial contamination. The antibacterial strategies that can turn water into things of value with high disinfection efficacy have been urgently needed for fuel system. Here, we reveal a water-fueled autocatalytic bactericidal pathway comprised by bi-metal micro-electrode system, which can spontaneously produce reactive oxygen species (mainly H_2O_2 and $O_2^{\bullet-}$) by the electron Fenton-like reaction in water medium without external energy., The respiratory chain component of bacteria and the galvanic corrosion on the coated metals were two electron sources in the system. The specific model of Ag-Ru water-fueled autocatalytic (WFA) microelectrode particles presents extremely high disinfection efficiency (>99.9999%) in less than one hour for three aerobic bacteria (*Escherichia coli*, *Pseudomonas aeruginosa* and *Bacillus subtilis*) in LB media and high disinfection efficiency for the anaerobic bacteria (*Desulfovibrio alaskensis*) in Postgate E media without natural light irradiation. Overall, the

* Corresponding authors.
E-mail addresses: ge@nwpu.edu.cn (Y. Ge), qi@nwpu.edu.cn (Z. Qi).

https://doi.org/10.1016/j.jhazmat.2022.129730
Received 23 June 2022; Received in revised form 1 August 2022; Accepted 6 August 2022
Available online 8 August 2022

novel WFA Ag-Ru antibacterial material explored in this study has a high potential for sterilizing applications in fuel system and this work provides the potential for the development of non-chemical and water-based antibacterial materials, such as WFA Ag-Ru antibacterial coating on stainless steel.

1. Introduction

Water is the most important constituent on Earth for all known forms of life. However, the existence of water under specific conditions, such as in the fuel system, can result in unexpected microbial contamination. Fuel biodeterioration has been recorded for more than 120 years since the first report by Miyoshi (Miyoshi, 1895; Passman, 2003, 2013; Gaylarde et al., 1999). Water is essential for microbial growth and always accumulated at the bottom of the fuel tank or pipe line. The American Society for Testing and Materials (ASTM) limits the free water and sediment content of diesel and biodiesel blends to 0.050 vol% (Shah et al., 2010). In addition to the water in the fuel, the amount of water in a fuel tank of aircraft changes with flight time, temperature, pressure, etc. Due to the suitable temperatures and sufficient nutrient sources present in fuel systems, microorganisms grow most actively at the water/fuel interface (Passman, 2003). According to previous research, the direct economic loss due to microbial corrosion is $30 to $50 billion per year (Xu et al., 2007) and there are more than 200 kinds of microorganisms that can grow in aviation fuel (Hu et al., 2018). Microbial contamination poses a significant threat to the aviation system security through mechanisms such as microbiologically influenced corrosion, fuel filter clogging, and fuel deterioration (Morton and Surman, 1994; Little and Lee, 2007). So the prevention and control of microbial contamination in fuel system is extremely important.

Common physical methods to minimize biological influences in fuel system include water removal, filtration, and heat treatment. The most recommended method to minimize the risk of biodegradation is water removal, but this is often easier said than done (Passman, 2013). It is difficult to remove water mechanically to avoid moisture accumulation and microbial growth. If the water in a fuel system could be converted to sterilization processes, it would greatly reduce the difficulty of inactivation and improve the efficiency of disinfection. Filtration and heating methods are used to remove microorganisms from the fuel or to kill microorganisms directly. However, the size of microorganisms is too small to filter out in fuel system, and heating fuel to high temperatures will cause the decomposition of fuel and affect fuel quality. In addition to the physical methods, biocide treatments are used as a strategy to prevent microbial contamination in fuel system (Passman, 2013). However, there are also many issues and limitations in the use of biocides, such as the lack of broad-spectrum activity, low chemical stabilities, negative influence to the environment (e.g. human and nature) and adverse effects on fuel system components (Toler, 1983; Hill and Hill, 2008). Therefore, it would be highly desirable to develop non-chemical and water-consuming disinfection technologies for fuel system conditions that can sterilize efficiently without compromising the fuel quality.

As is mentioned above, the disadvantages of physical and biocidal treatment methods restrict their bactericidal application in fuel system, so new antibacterial materials can be considered as an alternative sterilization strategy. Reactive oxygen species (ROS), such as hydrogen peroxide (H_2O_2), hydroxyl radicals (·OH) and superoxide anions ($O_2^{\bullet-}$), show a great bactericidal potential in an aqueous environment. Various techniques for generating ROS have been studied for the development of antibacterial materials in recent years. For examples, Fenton-like reaction has been extensively applied for producing ROS with H_2O_2 produced by two-electron oxygen reduction reaction ($2e^-$ ORR) in wastewater treatment (Huang et al., 2018, 2017; Pan et al., 2018; Yang et al., 2018). ROS can be also generated by metallic catalysts, an AgPd catalyst, during the synthesis of H_2O_2 from H_2 and O_2 for water disinfection (Richards et al., 2021). In addition, the photo-catalysis offers an alternative strategy for ROS generating. Many nanostructured photo-catalysts with high disinfection performances, such as MOFs (Dhakshinamoorthy et al., 2018; DeCoste and Peterson, 2014; Li et al., 2019; Chen et al., 2017a; Barea et al., 2014) and MoS_2 (Zhang et al., 2020; Chou et al., 2019; Meng et al., 2017; Liu et al., 2016), have been developed for disinfection purpose. However, these advanced strategies still require external energy inputs, such as light irradiation, electrical energy or heat transfer, which are difficultly delivered in fuel systems.

To realize the spontaneous release of ROS, the corrosion of metals can be an alternative and promising electron source for generating ROS autonomously. Several works (Vilela et al., 2017; Park et al., 2015, 2018) demonstrated the capacity of metal/metal oxide hybrids for disinfection performance. The electrons triggered by the corrosion process of degradable metal are transferred into the conduction bands of the metal oxide catalysis energetically and favorably. In this way, the H_2O_2 or other ROS can be generated spontaneously by the electrons in the metal oxide. The electron source for ORR can be also provided by the extracellular electron transfer (EET) in the aerobic bacteria, which has been proposed in microbial fuel cell (Kaila and Wikström, 2021). Some studies (Volentini et al., 2011; Rensing and Grass, 2003) have shown that the electron flow through the respiratory chain promotes cupric ions reduction in the vicinity of *Escherichia coli* (*E.coli*) surface. Electrons are donated by low-redox-potential electron donors such as NADH and transferred through a range of redox cofactors to the final electron acceptor (e.g., oxygen) (Wang et al., 2016). Up to now, a self-disinfecting surface triggered by galvanic corrosion and respiratory chain has rarely been introduced, particularly for reducing the risk of microbial contamination in fuel system.

Herein, a water-fueled autocatalytic (WFA) material comprising a bi-metal microelectrode (Ag and Ru) system was introduced that can produce ROS (mainly H_2O_2 and $O_2^{\bullet-}$) by electron (e^-)-Fenton-like reaction in a water medium without external stimulus. Silver ion itself has good bactericidal ability (Mei et al., 2017; Sharma et al., 2009; Carlson et al., 2008) and can form of small catalytic area with metals, such as Pd, Ru or Pt after specific treatment (Møller et al., 2007). Two electron sources for the electron e^--Fenton-like reaction, the respiratory chain component of bacteria and the galvanic corrosion on the coated metals, were verified by the electrochemical and fluorescence measurements. The disinfection efficiency of the WFA Ag-Ru particles against *Escherichia coli*, *Pseudomonas aeruginosa*, *Bacillus subtilis*, and the sulfate reducing bacterium *Desulfovibrio alaskensis* was more than 99.9999% in less than 2 h without natural light irradiation·H_2O_2 and $O_2^{\bullet-}$ are mainly responsible for the high broad-spectrum activity and outstanding inactivation performance. Additionally, the bi-metal system can be easily coated on differently shaped metal surfaces such as stainless steel (SS). SS with a WFA Ag-Ru coating also exhibited an excellent bactericidal activity without natural light irradiation at water/fuel interface, which has not been reported in previous studies. The system proposed in this study presents new concepts for WFA materials, reuses water as the antibacterial medium, and may provide new ideas for the development of efficient non-chemical and autocatalytic disinfection materials.

2. Materials and methods

2.1. Preparation of bi-metal microelectrode

In general, the WFA Ag-Ru microelectrode can be readily prepared by electrical/chemical deposition depending on the substrates (Ge et al., 2022). The technical details were described as followings:

a. WFA Ag-Ru microelectrode particle: One gram of freeze-dried Ag microparticles with a density of approximately 1 kg L^{-1} was suspended in 35 mL of ethylene glycol. Then, 17 mL of a 6.8 mM $RuCl_3$ solution and 6 mL of a 0.24 M sodium acetate solution were added. The color of the suspension changed from gray to greenish-brown. Then, 6 mL of a 0.6 M $NaBH_4$ solution was added dropwise under vigorous stirring, upon which the color changed to a deeper brown. The suspension was stirred for 30 min. Finally, the solutes were removed via extensive dialysis against deionized water.
b. WFA Ag-Ru coupon: A pure silver coupon with a 0.5 mm thickness was used as the substrate material, the surface of which was electrochemically plated with ruthenium. An Ag coupon was used as the working electrode with a working area of 10 mm × 10 mm, a saturated calomel electrode was used as the reference electrode, and a platinum sheet was used as the counter electrode. The electrolyte solution was 6.5 g L^{-1} $RuCl_3$ + 12 g L^{-1} sulfamic acid + 5 g L^{-1} NH_4Cl, the pH was approximately 3.0, and the temperature was 55 °C. The applied current density was 3 mA cm^{-2}, and the working time was 60 s. Magnetic stirring was carried out throughout the entire process. After reaction, the sample was rinsed by water extensively and dried.
c. Stainless-steel coupon with WFA Ag-Ru coating: A 304 L stainless-steel coupon with a 0.5 mm thickness was used as the substrate material, and silver and ruthenium were electrochemically plated onto the surface. The working area of the 304 L stainless-steel coupon was 10 mm × 10 mm, a saturated calomel electrode was used as the reference electrode, and a platinum sheet was used as the counter electrode. The solution used for coating silver was CT-361 purchased from Shenzhen Tianyue Chemical Industry, China. The applied current density, working time, pH, and temperature were 1 mA cm^{-2}, 60 s, 9.0, and room temperature, respectively. The solution for coating ruthenium was 6.5 g L^{-1} $RuCl_3$ + 12 g L^{-1} sulfamic acid + 5 g L^{-1} NH_4Cl, the pH was approximately 3.0, and the temperature was 55 °C. The applied current density was 3 mA cm^{-2}, and the working time was 60 s. Magnetic stirring was carried out throughout the entire process. After reaction, the sample was rinsed by water extensively and dried.

2.2. Characterization of the bi-metal microelectrode composition

The microstructure of the WFA Ag-Ru microelectrode particles was observed using field emission electron microscopy (FE-SEM) (MERLIN Compact Zeiss, Germany) equipped with energy dispersive X-ray spectrometry (EDS) and by transmission electron microscope (TEM, Talos-F200S, FEI, USA). Since the average diameter of the WFA Ag-Ru microelectrode particles was approximately 17.5 μm, an FIB (Tecnai G2-Twin F20, FEI, USA) was used to cut the samples for TEM.

The chemical composition of the synthetic WFA Ag-Ru microelectrodes was investigated using X-ray photoelectron spectroscopy (XPS). The XPS experiments were performed using an ESCALAB 250XI spectrometer (Thermo Fisher Scientific, USA). A monochromatic Al Kα radiation source was used for photoelectron emission, with a pass energy of 100 eV for the full spectra and 30 eV for the high-resolution spectra. The incident spot of the X-ray was 650 μm, the incident angle was 45°, and the vacuum chamber pressure was less than 1 × 10^{-7} Torr. The XPS results were analyzed using XPSPeak 4.1, and each peak was calibrated by the C1s peak (284.8 eV).

2.3. Oxygen reduction reaction performance

The electrochemical performance of the $2e^-$ ORR to H_2O_2 was studied using the rotating ring-disk electrode (RRDE) technique with a three-electrode cell system (Pizzutilo et al., 2017; Siahrostami et al., 2013). LSV was conducted in an O_2-saturated 0.1 M KOH solution with Ag/AgCl as the reference electrode and a platinum wire as the counter electrode. The working electrode was a silver electrode coated with ruthenium by electrochemical plating. An electrochemical workstation (CHI 760e, CH Instrument, China) was employed at a scan rate of 10 mV s^{-1} and rotating speeds of 400, 600, 900, 1200, and 1600 rpm. The potential applied to the disk was confirmed by CV of the materials (Fig. S6), and the potential applied to the ring was fixed at 1.2 V_{RHE}. The measured potentials were converted with respect to a reversible hydrogen electrode (RHE) and corrected for ohmic losses.

2.4. Bacterial current detection

The current-potential (*I-V*) curves were acquired from the samples on an electrochemical workstation (CHI 760e, CH Instrument, China) with LB broth electrolyte. The sample, platinum foil, and Ag/AgCl electrode served as the working electrode, counter electrode, and reference electrode, respectively. The applied potential range was set between − 0.3 and 0.2 $V_{Ag/AgCl}$ and the scan rate was 10 mV s^{-1}. The *I-V* curves were obtained with and without live/dead *E. coli.* The sample was 316 L SS coated with silver and ruthenium. For samples with live *E. coli* on the surface, 100 μL of the bacteria solution with a given concentration was dropped onto the sample surface and cultured at 37 °C for 30 min to form the biofilm. The samples were then covered with a micro-ester filter (0.45 μm) to prohibit the motility of bacteria to the electrolyte. The *E. coli* was sterilized by 75% ethanol for 30 min to obtain the dead cells. The experiments were repeated at least three times.

2.5. Disinfection efficacy of WFA Ag-Ru microelectrodes

Gram-negative *E. coli* (wild type), *P. aeruginosa* was isolated from a diesel pest (Erdmann et al., 2020), and gram-positive *B. subtilis* (Erdmann et al., 2020) was isolated from a diesel pest were used as reference bacteria under aerobic conditions. The sulfate-reducing bacterium *D. alaskensis* (AL1, DSMZ, Germany) was selected as an anaerobic model organism. The growth curves of the cultures were measured before the antibacterial experiments (Fig. S13). All the materials, tools, and chemicals were autoclave-sterilized prior to the experiments. For the aerobic experiments, the bacterial cells were incubated in LB medium (peptone 10 g L^{-1} + yeast 5 g L^{-1} + NaCl 5 g L^{-1}) at 37 °C overnight (16 h) to obtain a cell concentration of approximately 10^9 CFU mL^{-1}. For the *D. alaskensis* pre-culture, the cells were incubated in a nutrient solution of Postgate E (Stewart, 1984) (KH_2PO_4 0.5 g L^{-1}, NH_4Cl 1 g L^{-1}, Na_2SO_4 1 g L^{-1}, $CaCl_2.6\ H_2O$ 1 g L^{-1}, $MgSO_4.7\ H_2O$ 2 g L^{-1}, sodium lactate 3.5 g L^{-1}, yeast extract 1 g L^{-1}, ascorbic acid 0.1 g L^{-1}, thioglycolic acid 0.1 g L^{-1}, $FeSO_4.7\ H_2O$ 0.5 g L^{-1}, NaCl 0.5 g L^{-1}) at 37 °C for one week before use.

To distinguish the disinfection efficacy of WFA Ag-Ru and photocatalysts, the bacterial inactivation curves of the WFA Ag-Ru particles against aerobic bacteria with and without natural light irradiation were measured (Note: the natural light refers office fluorescent lamps (100 lm/W) with optical power density of 0.1 μW/cm^2, which is much less than 100 mW/cm^2 for sunlight). WFA Ag-Ru particles (0.5 mg mL^{-1}) and bacteria (3 ×10^6 CFU mL^{-1}) were added to 2 mL of LB medium. Two sets of experiments were conducted, one under natural light irradiation and the other under dark conditions. The number of living cells in the media was counted at different times using the standard flat colony counting method. Three types of aerobic bacteria, the gram-negative *E. coli*, *P. aeruginosa*, and the gram-position *B. subtilis* were used in this experiment. The concentration of WFA Ag-Ru particles was 0.5 mg mL^{-1}, and the process was the same as in the previous experiments.

To determine the disinfection efficacy of the WFA Ag-Ru coating at the water/fuel interface, 1 mL of aqueous medium and 1 mL of fuel were added to each tube and used as the solution for the next step. Bacteria at 3 × 10^6 CFU mL^{-1} were used as the initial cell concentration and incubated with and without a coupon coated with WFA Ag-Ru. The medium was then observed after incubation overnight.

2.6. Live/dead cell-staining

The damage to the bacterial cell membranes was detected by CLSM (TCS SP8 X LEICA, Germany) with a fluorescence model. One milliliter of overnight-cultured bacteria, 1 mL of fuel, and the WFA Ag-Ru sample were added to a tube and incubated for 3 h at 37 °C with a rotational shaking speed of 220 rpm. The suspensions were then centrifuged and washed with a 0.9% (w/v) NaCl, followed by staining with a LIVE/DEAD BacLight Bacterial Viability Kit (ThermoFisher Scientific, USA) according to the manufacturer's protocol. The experiment was performed using a mixture of SYTO 9 dye and propidium iodide dye. The live cells are stained by SYTO 9 and emit green fluorescence, whereas propidium iodide penetrates only damaged membranes and stains dead bacterial cells. After the light-protected incubation at room temperature for 15 min, the stained samples were observed by CLSM.

2.7. ROS measurements

H_2O_2 detection was performed using a fluorescence probe. A fluorescent dimer forms by the reaction of H_2O_2 with HPA using horseradish peroxidase as a catalyst. The amount of the dimer was analyzed using a fluorescence spectrophotometer at an emission wavelength of 410 nm with excitation at 315 nm. ·OH radicals were measured by detecting the fluorescent products generated by coumarin (Cou), ·OH. Cou (0.1 mM) and WFA Ag-Ru particles (1 mg mL^{-1}) were dispersed in an aqueous solution. The fluorescence spectra of OH-Cou were recorded at an emission wavelength of 455 nm with excitation at 332 nm. The $O_2^{\bullet-}$ steady-state concentration was calculated by measuring the decay of nitroblue tetrazolium (NBT) (Sigma, 98%) using UV–vis spectroscopy. NBT exhibits an absorption peak at 260 nm, and the rate constant for the $O_2^{\bullet-}$ and NBT reaction is 5.9×10^4 M^{-1} s^{-1} (Li et al., 2019; Liu et al., 2016).

2.8. Scavenger quenching experiments

The employed scavengers were catalase (300 U mL^{-1}, Sigma) for H_2O_2, isopropanol (2.5 mM, Sigma, 99.5%) for·OH, superoxide dismutase (400 U mL^{-1}, Sigma, 99%) for $O_2^{\bullet-}$, $_L$-histidine ($_L$-His, 2.5 mM, Sigma, 99%) for $^1O_2$, sodium chromate (Cr(VI)), 2.5 mM, Sigma, 99.5%) for electrons, and sodium oxalate (2.5 mM, Sigma, 99.5%) for holes (Li et al., 2019). The bacteria were pre-cultured in triplicate at 37 °C overnight (16 h) with a rotational shaking speed of 220 rpm. Then, the bacteria grown in LB medium were added to a 2 mL centrifuge tube at a concentration of 3×10^6 CFU mL^{-1}. The WFA Ag-Ru particles (0.5 mg mL^{-1}) and scavengers were added to the bacterial suspension separately before incubation. The number of bacterial cells in the media was counted at different times using the standard flat colony counting method. The empirical Chick–Watson equation was used to calculate the disinfection kinetics:

$$\ln\frac{C}{C_0} = -k\delta^m t, \tag{1}$$

where C_0 and C are the initial and subsequent bacterial concentrations, respectively, t is the experimental time, k is the disinfection kinetic constant, δ is the concentration of particles, and m is the order of the reaction.

3. Results and discussion

3.1. Material characterization of WFA Ag-Ru particles

The WFA Ag-Ru material can be readily prepared by electrical/chemical deposition. Supplementary Materials described the detailed fabrication process on diverse commercial available substrates. Macroscopically, the WFA Ag-Ru particles appeared as a fine gray powder due to the presence of ruthenium (Fig. 1a). The microstructure of the WFA Ag-Ru powder was observed by field emission electron FE-SEM with elemental analysis by EDS. As displayed in Fig. 1b and c, the powder consisted of microparticles with a diameter of approximately 17.5 μm. According to the elemental mapping analysis, silver and ruthenium were well distributed on the surface of every particle with atomic percentages of 2–3% and 30–40%, respectively. Because the interior of the solid particles consisted of SiO_2, the balanced elements were mainly Si and O, and the thickness of the silver and ruthenium layers was less than 100 nm (Fig. S1). The TEM observations of a particle cut with a focused ion beam (FIB) (Fig. 1f–h and S2–S5) showed that the silver layer was much thicker than the ruthenium layer on the surface. The outermost layer was mainly platinum with a thickness of approximately 20 nm, which was used to protect the sample surface during the FIB cutting process. The silver layer, which was close to the interior SiO_2 particle, was compact with a thickness of approximately 100 nm. The ruthenium layer covered the silver layer with a thickness of approximately 10 nm. The same TEM observation was performed for a silver coupon with a ruthenium coating (Figs. S2–S5). The elemental mapping results indicated that silver and ruthenium thoroughly covered the surfaces of the particles and were well mixed.

To analyze the valence states of silver and ruthenium on the surface of the WFA Ag-Ru particles, the XPS technique was applied. The metallic and oxidized states of Ag 3d and Ru 3d are shown in Fig. 1e, respectively. According to the binding energies in the NIST database, two kinds of valence state of silver, Ag (368.2 and 374.2 eV) and Ag^+ (367.8 and 373.8 eV), were shown by fitting the Ag 3d plot. There is a very strong overlap between the Ru 3d and C 1 s regions, so the curve of Ru 3p was used to analysis the ruthenium. The Ru 3p spectra were split into four peaks corresponding to Ru (461.8 and 484.3 eV) and Ru^{4+} (464.9 and 486.7 eV).

3.2. ORR performance of WFA Ag-Ru microelectrodes and theoretical studies

To verify the occurrence of the $2e^-$ ORR in the WFA Ag-Ru system, RRDE electrochemical method was applied with a silver electrode as a control. The H_2O_2 selectivity can be calculated from the current density of O_2 reduction at the disk and of H_2O_2 oxidation at the ring of the RRDE. Taking into consideration that the disk current density (i_{Disk}) is the sum of the O_2 reduction current densities to water (i_{H2O}) and H_2O_2 (i_{H2O2}), $i_{Disk} = i_{H2O} + i_{H2O2}$, and using the ring current densities (i_{Ring}) and collection efficiency N of the ring current density, $i_{H2O2} = i_{Ring} N^{-1}$, the selectivity for H_2O_2 generation (H_2O_2%) can be calculated from the ratio between the O_2 consumption rate toward H_2O_2 and the total consumption rate (Paulus et al., 2001; Jiang et al., 2018).

$$H_2O_2\% = 200 \times \frac{i_{Ring}/N}{i_D + i_{Ring}/N} \tag{2}$$

The collection efficiency (N) was 32.89% as determined from measurements of hexacyanoferrate(III) reduction. The number of electrons transferred for the ORR, n, can be calculated from

$$n = 4 \times \frac{i_D}{i_D + i_{Ring}/N}. \tag{3}$$

The yield of H_2O_2 corresponds to the current density of the ring. The ring current density (Fig. 2a) was notably higher on the WFA Ag-Ru microelectrodes than on a silver electrode, indicating that the $2e^-$ ORR process occurred in the WFA Ag-Ru system. As calculated by Eqs. (2) and (3) (Fig. 2b), the electron transfer number of the WFA Ag-Ru microelectrodes was 3.2–3.6, and the H_2O_2 selectivity approached 40%, which is 5–19 times higher than that of the silver electrode. The results of the RRDE analysis at different rotating speeds reached similar conclusions (Fig. S7). Clearly, the $2e^-$ ORR occurs when ruthenium is combined with silver, and considerably more H_2O_2 can be generated

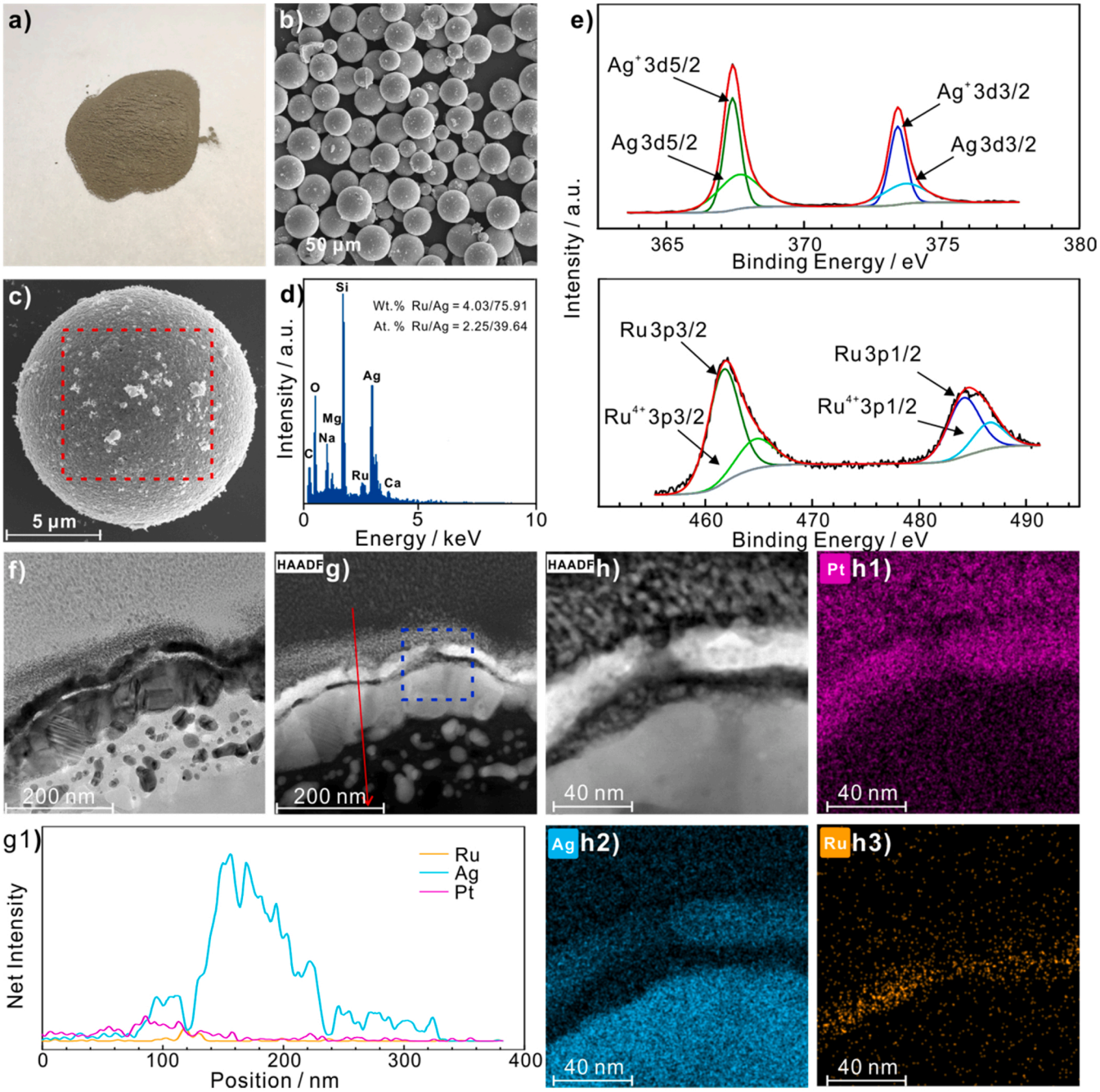

Fig. 1. Characteristics of WFA Ag-Ru microelectrode particles. a) Macroscopic features observed by optical microscopy. b, c) SEM microstructure at different magnifications. d) EDS profile of the area in the red square in c). e) Ru and Ag elemental XPS results of WFA particles. f) TEM image of a single particle after FIB cutting. g) HAADF-STEM image and g1) STEM-EDS line-scanning profile of the red line in g). h) Higher magnification HAADF-STEM image of the area in the blue square in g). h1–h3) STEM-EDS mapping images, where purple is Pt, blue is Ag, and yellow is Ru.

compared with the silver electrode. The work function of ruthenium is higher than that of silver, which means that removing electrons from the former is more difficult. When silver and ruthenium are in contact, a contact potential difference (galvanic corrosion) occurs, and silver acts as an electron donor, allowing the $2e^-$ ORR to proceed spontaneously. The durability of the WFA Ag-Ru microelectrodes was also examined using the RRDE experiment (Fig. 2c). The H_2O_2 selectivity remained high even after 36 h of use. The ORR activity can be compared using the half-wave potential $E_{1/2}$ from the LSV results shown in Fig. 2a. The half-wave potential $E_{1/2}$ of the silver electrode (0.71 V_{RHE}) was 160 mV higher than that of WFA Ag-Ru (0.56 V_{RHE}), indicating that the ORR activity of silver is higher. This is because the electrical conductivity of ruthenium is lower than that of silver. The CV curves of the two electrodes are shown in Fig. S6.

The Gibbs free energy change of silver combined with ruthenium during the $2e^-$ ORR was studied by DFT calculations. The $2e^-$ ORR requires two steps to reduce O_2 to H_2O_2 and involves one intermediate, OOH* . The first step is $O_2 + * + H^+ + e^- \rightarrow OOH^*$, and the second is $OOH^* + H^+ + e^- \rightarrow H_2O_2 + *$. The Gibbs free energies of adsorption ($\triangle G_{ads}$) during these two steps are shown in Fig. S9 for Ag(111) with different Ru doping densities. When the atomic ratio of Ru to Ag was 1:15, $\triangle G_{ads}$ of each step (4.49 and 1.99 eV, respectively) was the lowest, indicating that this ratio is the most likely to generate H_2O_2. When the atomic ratio of Ru to Ag was high (1:3 and 1:1), $\triangle G_{ads}$ of each

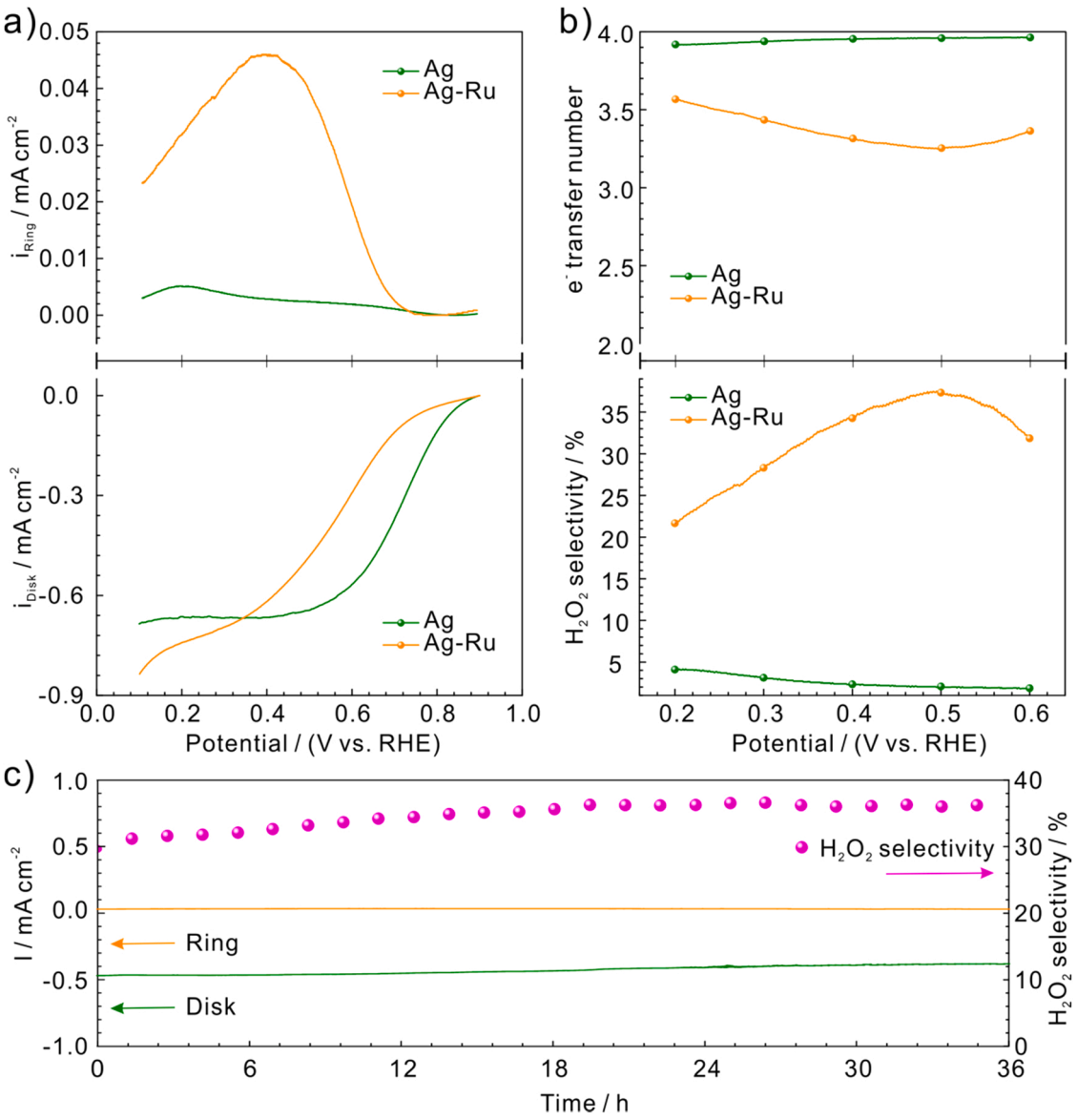

Fig. 2. ORR performance of Ag electrode and WFA Ag-Ru microelectrode particles investigated by RRDE experiments in oxygen-saturated 0.1 M KOH. a) Linear sweep voltammetry (LSV) of Ag and WFA Ag-Ru and detected H_2O_2 currents on a ring electrode at a fixed potential of 1.2 V_{RHE}. b) H_2O_2 selectivity and electron transfer number with respect to the potential applied to different electrodes. The LSV experiments were recorded at a rotating speed of 1600 rpm and scan rate of 10 mV s^{-1}. c) Stability measurement of WFA Ag-Ru microelectrodes with a fixed disk potential of 0.4 V_{RHE} and ring potential of 1.2 V_{RHE}.

step was higher than that of Ag. As a prototypical model, we built an Ru-doped system on Ag(111) with different doping densities. The system exhibited the highest H_2O_2 activity and selectivity when the atomic ratio (Ru:Ag) was 1:15, which was close to the atomic ratio of the WFA Ag-Ru microelectrodes. The models of Ag(111) with different Ru doping densities are shown in Fig. S8.

3.3. Fenton-like reaction and disinfection efficacy of WFA Ag-Ru particles

H_2O_2 was further detected by the fluorescence method using *p*-hydroxyphenylacetic acid (HPA) as an H_2O_2 probe (Li et al., 2019; Nosaka and Nosaka, 2017). The experiments were performed with 2 mg mL^{-1} WFA Ag-Ru particles in water (1 mL) for 60 min. The concentration of generated H_2O_2 was 0.76 μM, (Fig. 3a and S10d), and 5 μM $O_2^{\bullet-}$ was generated as determined by the NBT reduction approach (Fig. 3b and S10e). The existence of·OH was confirmed using coumarin (Cou) as a probe (Fig. 3c and S10f), by which the·OH yield was determined as 10^{-3} μM.·OH can also be generated by silver when H_2O_2 is added to the system (Fig. S11). The presence of ROS proves that a Fenton-like reaction occurs in the WFA Ag-Ru system.

The bactericidal performance of the WFA Ag-Ru particles was examined against *E. coli* at an initial concentration of 3×10^6 CFU mL^{-1} in LB medium at particle dosages of 0.01, 0.1, and 0.3 mg mL^{-1} (Fig. 3d). The WFA Ag-Ru particles displayed antibacterial effect when the dosage reached 0.01 mg mL^{-1}, which meant the minimum inhibitory concentration (MIC) value was 0.01 mg mL^{-1}. The MIC value of the WFA Ag-Ru particles is smaller than most of the bimetallic bactericidal material reported before, such as bimetallic Zn-Ag-NaY zeolite (Ferreira et al., 2016), AgCu-Y zeolite (Ferreira et al., 2015), Cu/Zn montmorillonites (Jiao et al., 2017), and some bimetallic nanoparticles (Bakina et al., 2019; Andrade et al., 2017; Cai et al., 2017), etc. The WFA Ag-Ru particles showed an excellent bactericidal activity and reached almost complete disinfection (>99.9999% disinfection efficiency) of *E. coli* at a particle concentration of 0.1 mg mL^{-1} after 180 min of incubation. The time for complete disinfection was shortened to 120 min by increasing the particle concentration to 0.3 mg mL^{-1}. Guridi et al (Guridi et al.,

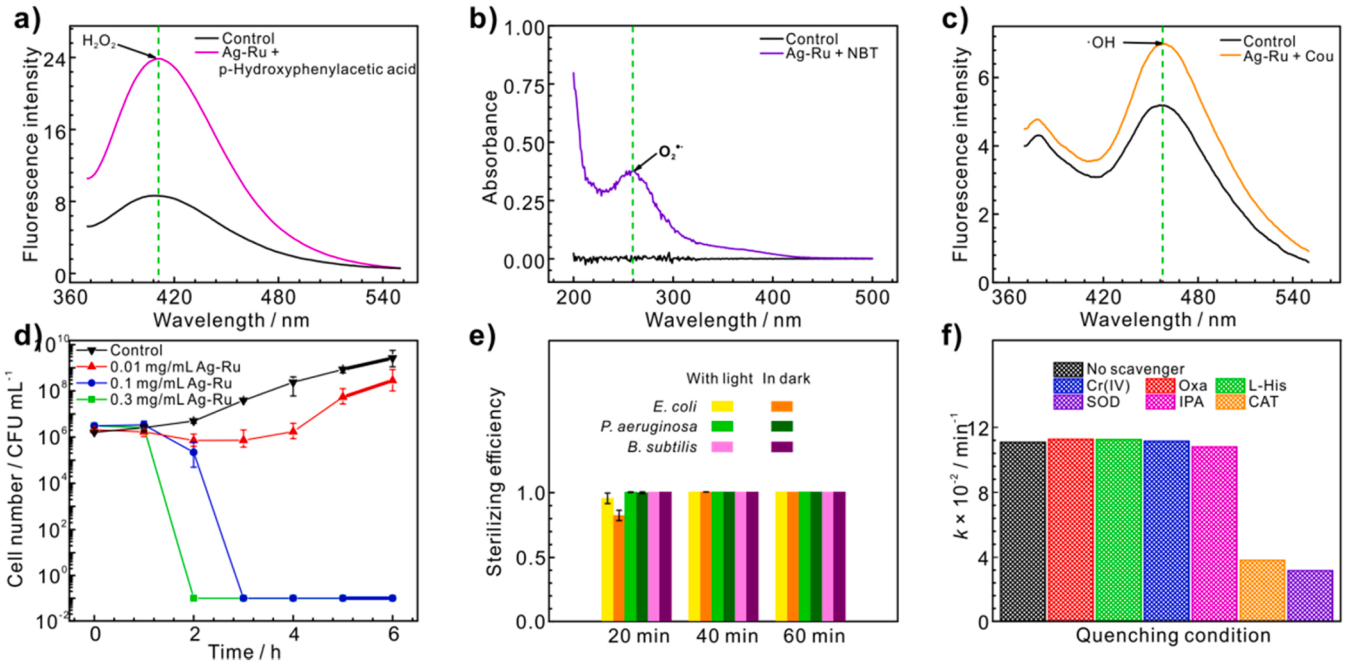

Fig. 3. a) H_2O_2 detected by fluorescence using HPA as a fluorescent probe. b) $O_2^{\bullet-}$ verified by the decay of NBT using UV–vis spectroscopy. c)·OH confirmed by fluorescence spectroscopy using Cou as a fluorescence probe. d) Bacterial inactivation assay of different dosages of WFA Ag-Ru microelectrodes against *E. coli*. The initial bacterial number was 3×10^6 CFU mL^{-1}; the number of bacteria was recorded once every hour. e) Sterilizing efficiency (SE) of WFA Ag-Ru microelectrodes for different kinds of bacteria with and without natural light irradiation. f) First-order disinfection rate on WFA Ag-Ru particles with different scavengers (IPA →·OH, OXA → h^+, Cr(IV) → e^-, L-his → 1 O^2, CAT → H_2O_2, SOD →$O_2^{\bullet-}$). The error bars were calculated via repeating the measurements three times.

2015). reported the disinfection performance of one similar commercial material AgXX® coating and the results revealed a reduction amounting to a decrease of 10^3 CFU mL^{-1} (equals to 99.9% disinfection efficiency) in the presence of AgXX®. The WFA Ag-Ru particles showed higher disinfection efficiency than the similar material AgXX®. In addition, the antibacterial efficiency of the WFA Ag-Ru particles than other autocatalytic materials, such as Au@TiO_2 nanoparticles (Wang et al., 2016) (80% antibacterial efficiency at 1 h) and Au@ZnO nanoparticles (Wang et al., 2020) (80% antibacterial efficiency at 24 h). The results of the bacteriostatic zone test for Ag particles and WFA Ag-Ru particles also indicated that the WFA Ag-Ru microelectrodes exhibit a better disinfection performance than the silver electrode (Fig. S14). Moreover, the evidently better disinfection performance was observed on SS coupon coated with Ag-Ru against with *E. coli* than the SS coupon coated with Ag and the SS coupon. The morphologies of the *E.coli* cells on the three kinds of coupon were shown in Fig. S15. The disinfection efficacy of the WFA Ag-Ru particles is comparable to that of some recently developed photocatalytic materials under natural light or UV-light irradiation (Li et al., 2019; Liu et al., 2016).

To verify that the disinfection performance of the WFA Ag-Ru particles is independent of natural light irradiation, inactivation experiments were conducted under light-protected conditions and with natural light irradiation. The outstanding disinfection efficacies of the WFA Ag-Ru particles regardless of natural light irradiation are exhibited in Fig. 3e and S16, and the data were shown in Table 1. Meanwhile, the complete disinfection time at the same particle dosage was different for different cultures, e.g., 20 min for *B. subtilis* versus 60 min for *E. coli*. The disinfection performance of the WFA Ag-Ru microelectrode was comparable to some photocatalytic bactericidal materials. Li et al (Li et al., 2019). reported a zinc-imidazolate MOF (ZIF-8) which exhibited almost complete inactivation of *E. coli* (>99.9999% inactivation efficiency) in saline within 2 h of simulated solar irradiation. Liu et al (Liu et al., 2016). reported a few-layered vertically aligned MoS_2 (FLV-MoS_2) film which achieved water disinfection of > 99.999% inactivation of bacteria in 20 min with a small amount of material (1.6 mg L^{-1}) under simulated visible light. However, unlike photocatalytic bactericidal materials, the WFA Ag-Ru microelectrodes are light independent and have an enormous advantage when applied in a light-protected environment.

To determine the dominant bactericidal substance in the WFA Ag-Ru system, scavenger quenching experiments were conducted. The disinfection rate shown in Fig. 3 f was calculated from the bacterial inactivation curves with and without a specific scavenger (Fig. S17). The scavenger quenching results shown in Fig. 3 f indicate that H_2O_2 exhibited the strongest bactericidal effect, with $O_2^{\bullet-}$ showing the second strongest. Therefore, H_2O_2 and $O_2^{\bullet-}$ are the main species responsible for the excellent disinfection performance of the WFA Ag-Ru system. As H_2O_2 was generated by 2e$^-$ ORR, so the disinfection performance can be future improved by increasing H_2O_2 selectivity and 2e$^-$ ORR activity of WFA bi-metal material, which may be achieved by optimizing the ratio of bi-metal and adjusting the specific surface area.

Table 1
The sterilizing efficiency (SE) of WFA Ag-Ru microelectrodes for different kinds of bacteria with and without natural light irradiation.

Bacteria	*E.coli*		*P. aeruginosa*		*B. subtilis*	
SE	Light	Dark	Light	Dark	Light	Dark
20 min	95.0000%	81.8181%	99.6250%	99.3010%	99.9999%	99.9999%
40 min	99.9999%	99.9200%	99.9999%	99.9999%	99.9999%	99.9999%
60 min	99.9999%	99.9999%	99.9999%	99.9999%	99.9999%	99.9999%

3.4. Electron sources for WFA Ag-Ru bi-metal self-disinfection system

Two hypotheses of the electron sources for above-mentioned ORR were proposed, galvanic corrosion and extracellular electron transfer (EET). The galvanic corrosion generally occurs when two metals (e.g. Ag and Ru) are in direct contact in an electrolyte, and then the electron transfers from the more reactive metal to the less reactive one through the electrolyte (Ge et al., 2022). It is widely accepted that chloride ion is a kind of corrosive ion for metal (Chen et al., 2017b; Berrocal et al., 2016; Ni et al., 2017), which can accelerate galvanic corrosion. Therefore, the generation of H_2O_2 triggered by galvanic corrosion in WFA Ag-Ru self-disinfection system was consequently studied and confirmed in the electrolyte with different chloride ion densities by electrochemical measurement (Fig. 4b and c). Indeed, the fluorescence intensity increased of H_2O_2 when adding more chloride ions into the electrolyte (Fig. 4b), which meant the chloride ions accelerated the galvanic corrosion between silver and ruthenium and improved the yield of H_2O_2 (Fig. 4c).

The potential EET between *E. coli* and stainless steel coupons coated with WFA Ag-Ru was also investigated and verified by electrochemical method. *I-V* curves of the samples with different conditions were shown in Fig. 4d and e. When live *E. coli* was added into the electrolyte, the response current was increased. This phenomenon supported the EET occurred at the interface between sample and bacteria. We speculate that the live *E. coli* cells may act similarly as light illumination in localized surface plasmon resonance (LSPR) excitation and supply hot electrons to produce the bacterial current (Wang et al., 2020). The *I–V* curves are assessed vertically during the antibacterial process (Fig. 4d) and horizontally with different amounts of original live bacteria (Fig. 4e). The saturation current dropped and the triggering voltage increased when the interaction time between samples and *E. coli* was increased, which implied that the generation of bacterial current became more difficult as more bacteria were inactivated. Moreover, when the live bacteria concentration was increased, the triggering voltage decreased and the saturation current increased, indicating that the EET was enhanced by more interaction between bacteria and samples.

3.5. Inactivation properties of WFA Ag-Ru coating at water/fuel interface

To prove that the WFA Ag-Ru system can also be used as an antibacterial coating in light-protected fuel systems, silver and ruthenium were electrochemically plated on the surface of 316 L stainless steel, and the inactivation properties were examined at the water/fuel interface. Because the fuel system may also lack oxygen, three types of aerobic bacteria and one anaerobic bacterium were chosen as test cultures. The aerobic bacteria were incubated for 16 h and the anaerobic bacteria (due to the higher generation time) for one week at 37 °C. Then, the coupon with the Ag-Ru coating was set in new medium (the volume ratio between nutrient solution and fuel as 1:1) and incubated for 3 h (aerobic) and 4 d (anaerobic) at 37 °C. The live/dead cells were observed by confocal laser scanning microscopy (CLSM), and the results are shown in Fig. 5. For the aerobic cultures, the coupon with the WFA Ag-Ru coating exhibited remarkable disinfection ability, and the cells were almost completely damaged. Without the coated coupon, very few dead cells were observed according to the normal growth to death phase. For the anaerobic culture with the coated coupon, not all the cells were killed, as some live cells (shown in green color) could be found (Fig. 5). Because of the lack of oxygen under anaerobic conditions, no ORR or Fenton-like reaction occurs, and thus no H_2O_2 or other ROS is generated by the WFA Ag-Ru coating. In this case, the disinfection efficacy arises mainly from the released silver ions in the medium. The released silver ions from different types of samples in the system were examined by inductively coupled plasma mass spectrometry (ICP-MS). The results showed that the released Ag^+ concentration was 469 ppb for WFA Ag-Ru microelectrode particles, 1310 ppb for WFA Ag-Ru coupon, 842 ppb for Ag coupon, and 1818 ppb for the stainless steel with WFA Ag-Ru coating after 72 h of immersion (Fig. S12). The minimum inhibitory concentration of silver ions been estimated to 30–125 ppb, and the necessary concentration for full killing effect (minimum bactericidal concentration, MBC) 480–1005 ppb (Møller et al., 2007). So the WFA Ag-Ru coupon and the stainless steel with WFA Ag-Ru coating can

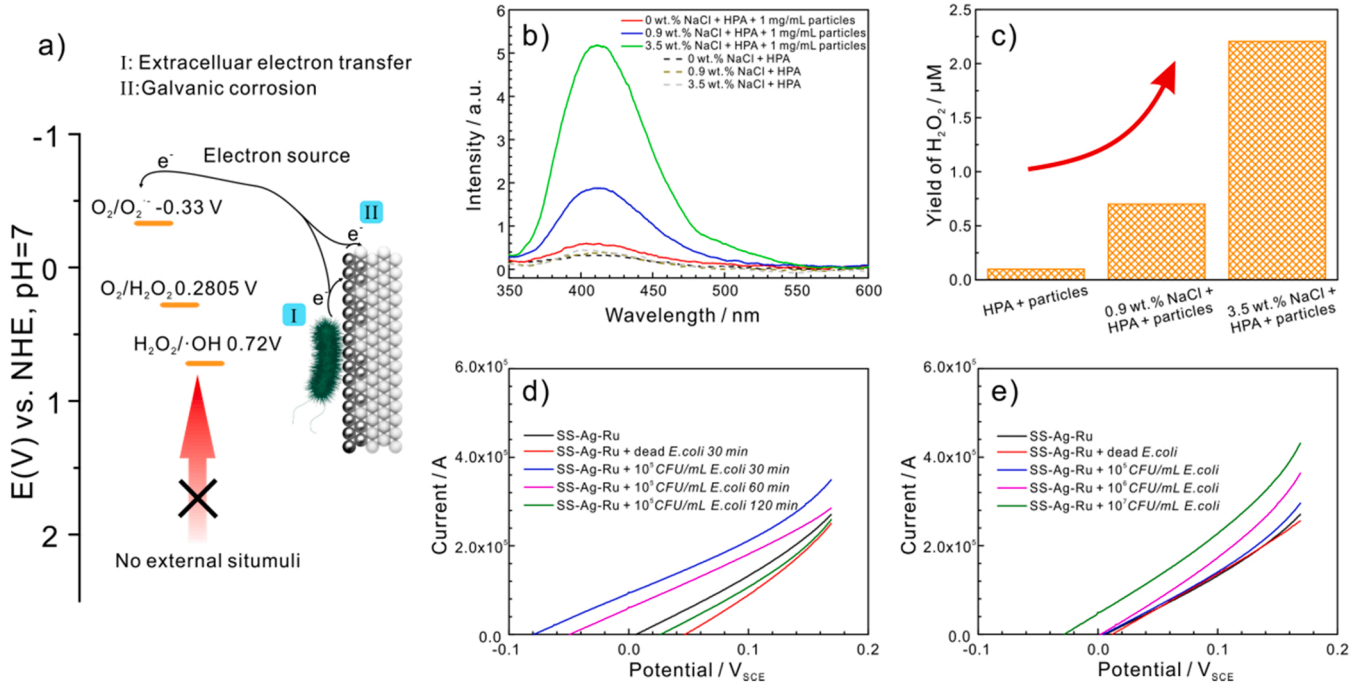

Fig. 4. a) Schematic diagram illustrating two electron sources in WFA Ag-Ru bi-metal self-disinfection system. b) Detection of H_2O_2 in the system with different Cl^- concentrations by fluorescence. c) Yield of H_2O_2 in the system with different Cl^- concentrations. d) *I-V* curves of 316 L stainless steel coated with WFA Ag-Ru interacting with bacteria for different duration time. e) *I-V* curves of the samples with different amounts of bacteria on the surface, the duration time was 30 min.

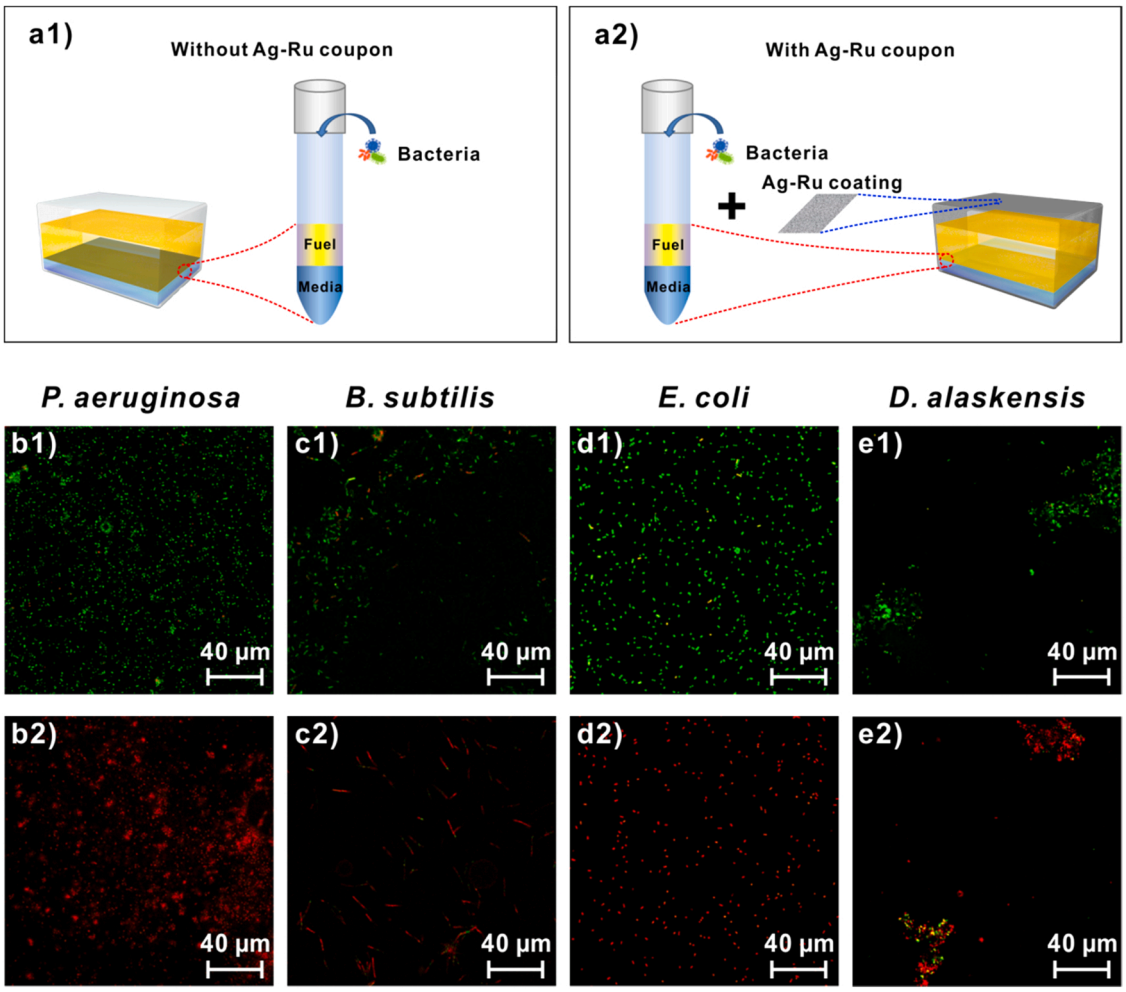

Fig. 5. a) Sketch of disinfection at water/fuel interface with and without WFA Ag-Ru coating. CLSM observation of live/dead b) *P. aeruginosa*, c) *B. subtilis*, d) *E. coli*, and e) *D. alaskensis* cells. Green: live cells; Red: dead cells. Under aerobic conditions, the three cultures were killed completely by the WFA Ag-Ru coupon, with the WFA Ag-Ru microelectrodes showing an excellent and rapid disinfection performance. Under anaerobic conditions, most of *D. alaskensis* was killed, with the WFA Ag-Ru microelectrodes displaying an ordinary disinfection capability. The area was 200 μm × 200 μm.

sterilize the bacteria by released silver ions after a long time immersion (more than 3 days) even in an anaerobic environment. The disinfection performance of the WFA Ag-Ru coupon against the anaerobic bacterium *D. alaskensis* is shown in Fig. S19. Although the concentration of released silver ions was not high enough to reach the minimum bactericidal concentration, the ions could still kill the bacteria after long-term immersion as mentioned above. Hence, the WFA Ag-Ru coating can be applied in fuel systems, although the disinfection efficiency is slightly lower in the absence of oxygen. Control experiments for the inactivation properties of a stainless-steel coupon and silver coupon were also carried out (Fig. S18). Only the silver coupon showed a weak disinfection efficacy against *B. subtilis*.

4. Conclusion

In summary, we explored the disinfection efficacy of a WFA material comprising silver and ruthenium bi-metal microelectrodes that can potentially be used as an antibacterial material in fuel systems. Regardless of light irradiation, the WFA Ag-Ru particles show an outstanding disinfection performance. Two electron sources for the e-Fenton like reaction, the respiratory chain component of bacteria and the galvanic corrosion on the coated metals, were verified by the electrochemical and fluorescence measurements. Under aerobic conditions, the e-Fenton-like reaction can proceed spontaneously to generate ROS. Due to the excellent disinfection ability of H_2O_2 and $O_2^{\bullet-}$, the WFA Ag-Ru particles exhibit a remarkable disinfection efficacy. In the absence of oxygen, silver ions released from WFA Ag-Ru are responsible for the inactivation efficiency. We will investigate how the biocidal effect of WFA material can be improved for the anaerobic conditions. However, the clear effect under aerobic conditions can be already beneficial for a broad range of industry infrastructures. Moreover, the utilization of water and oxygen, which are hazardous fuel system components, in the disinfection process will significantly increase the safety factor of fuel systems. The WFA Ag-Ru coating on stainless steel provides strong and comprehensive protection against bacteria in the fuel system. This work also offers valuable ideas for the development of high-efficiency, environmental-friendly and water-consuming autocatalytic antibacterial materials.

Environmental implications

Microbial contamination is an unavoidable and crucial problem in industrial environment, which may cause a great economic loss and life threat. The water-fueled autocatalytic bi-metal bactericidal pathway can spontaneously produce ROS for efficient disinfection by the electron Fenton-like reaction without external energy. Extracellular electron transfer and galvanic corrosion processes act as the electron sources in the system. This work provides a green and efficient antibacterial

strategy and has a high potential for sterilizing applications in the closed, dark and damp environment, such as the fuel system.

CRediT authorship contribution statement

Jizheng Yao: Methodology, Data curation, Writing – original draft, Writing – review & editing. **Tao Jiang:** Methodology. **Yucheng Ji:** Methodology. **Biwen Annie An:** Methodology, Data curation, Writing – review & editing. **Andrea Koerdt:** Methodology, Data curation, Writing – review & editing. **Zhongqi Cai:** Methodology. **Chaofang Dong:** Methodology, Data curation. **Yan Ge:** Conceptualization, Methodology, Writing – review & editing, Project administration. **Zhenhui Qi:** Conceptualization, Writing – review & editing, Supervision, Project administration.

Declaration of Competing Interest

The authors declare the following financial interests/personal relationships which may be considered as potential competing interests: Zhenhui Qi reports financial support was provided by Northwestern Polytechnical University. Zhenhui Qi reports a relationship with Northwestern Polytechnical University that includes: employment. Zhenhui Qi has patent pending to PA21047330 patent filing. None.

Data Availability

Data will be made available on request.

Acknowledgments

We gratefully acknowledge financial support from the National Natural Science Foundation of China (52001255, 22071196, 22007078), Key Research and Development Program of Shaanxi Province (2021KWZ-18), Aeronautical Science Foundation of China (ASFC-2020Z061053001), Opening Project of State Key Laboratory of Polymer Materials Engineering (Sichuan University) (Grant No. klpme2021–05-03), Student Innovation and Entrepreneurship Education Center of the Student Work Department of the Party Committee of NPU (2021-cxcy-012), Higher Education Research Fund of NPU (CJGZMS202202), the Fundamental Research Funds for the Central Universities, and Fellowship from CSC Innovative Team Program (CXXM20190099, CXXM2110141862). We thank the Analytical & Testing Center of NPU for the characterization of materials. We also thank the BAM group members (Dr. Frank Schreiber, Dr. Niclas Nordholt, Selina Schmidt and Gabriel Heidrich) of Dr. Frank Schreiber for their assistances and suggestions in the experiments on microbiology. We are also grateful to Ms. Sherin Kleinbub for providing the diesel strains and Mr. René Hesse for FIB analysis.

Appendix A. Supporting information

Supplementary data associated with this article can be found in the online version at doi:10.1016/j.jhazmat.2022.129730.

References

M. Miyoshi, Die durchbohrung von membranen durch pilzfäden, 1895.
Passman, F.J., 2003. Introduction to fuel microbiology. Manual 1e13.
Passman, F., 2013. Microbial contamination and its control in fuels and fuel systems since 1980–a review. Int. Biodeterior. Biodegrad. 81, 88–104.
Gaylarde, C.C., Bento, F.M., Kelley, J., 1999. Microbial contamination of stored hydrocarbon fuels and its control. Rev. De. Microbiol. 30, 01–10.
Shah, P., Wee, C., White, J.M., Sanford, S., Meier, G., 2010. Experimental determination and thermodynamic modeling of water content in biodiesel-diesel blends. Renew. Energy Group.
Xu, C., Zhang, Y., Cheng, G., Zhu, W., 2007. Localized corrosion behavior of 316L stainless steel in the presence of sulfate-reducing and iron-oxidizing bacteria. Mater. Sci. Eng.: A 443, 235–241.
D. Hu, J. Han, R. Zhang, Y. Zhang, Y. Xing, X. Zhao, M. Li, Control of Microbial Contamination in Aircraft Fuel System, (2018).
Morton, L., Surman, S., 1994. Biofilms in biodeterioration—a review. Int. Biodeterior. Biodegrad. 34, 203–221.
Little, B.J., Lee, J.S., 2007. Microbiologically influenced corrosion. John Wiley & Sons.
J. Toler, The use of biocides for improving storage conditions of fuels, in: Conference on Long Term Storage Stabilities of Liquid Fuels, Tel Aviv, Israel, 11e14 July, 1983, pp. D42eD50.
Hill, E.C., Hill, G.C., 2008. Microbial contamination and associated corrosion in fuels, during storage, distribution and use. In: Advanced Materials Research. Trans Tech Publ, pp. 257–268.
Huang, B.-C., Jiang, J., Wang, W.-K., Li, W.-W., Zhang, F., Jiang, H., Yu, H.-Q., 2018. Electrochemically catalytic degradation of phenol with hydrogen peroxide in situ generated and activated by a municipal sludge-derived catalyst. ACS Sustain. Chem. Eng. 6, 5540–5546.
Pan, Z., Wang, K., Wang, Y., Tsiakaras, P., Song, S., 2018. In-situ electrosynthesis of hydrogen peroxide and wastewater treatment application: A novel strategy for graphite felt activation. Appl. Catal. B: Environ. 237, 392–400.
Huang, B., Qi, C., Yang, Z., Guo, Q., Chen, W., Zeng, G., Lei, C., 2017. Pd/Fe3O4 nanocatalysts for highly effective and simultaneous removal of humic acids and Cr (VI) by electro-Fenton with H2O2 in situ electro-generated on the catalyst surface. J. Catal. 352, 337–350.
Yang, S., Verdaguer-Casadevall, A., Arnarson, L., Silvioli, L., Čolić, V., Frydendal, R., Rossmeisl, J., Chorkendorff, I., Stephens, I.E., 2018. Toward the decentralized electrochemical production of H2O2: a focus on the catalysis. ACS Catal. 8, 4064–4081.
Richards, T., Harrhy, J.H., Lewis, R.J., Howe, A.G., Suldecki, G.M., Folli, A., Morgan, D. J., Davies, T.E., Loveridge, E.J., Crole, D.A., 2021. A residue-free approach to water disinfection using catalytic in situ generation of reactive oxygen species. Nat. Catal. 4, 575–585.
Dhakshinamoorthy, A., Li, Z., Garcia, H., 2018. Catalysis and photocatalysis by metal organic frameworks. Chem. Soc. Rev. 47, 8134–8172.
DeCoste, J.B., Peterson, G.W., 2014. Metal–organic frameworks for air purification of toxic chemicals. Chem. Rev. 114, 5695–5727.
Li, P., Li, J., Feng, X., Li, J., Hao, Y., Zhang, J., Wang, H., Yin, A., Zhou, J., Ma, X., 2019. Metal-organic frameworks with photocatalytic bactericidal activity for integrated air cleaning. Nat. Commun. 10, 1–10.
Chen, Y., Zhang, S., Cao, S., Li, S., Chen, F., Yuan, S., Xu, C., Zhou, J., Feng, X., Ma, X., 2017a. Roll-to-roll production of metal-organic framework coatings for particulate matter removal. Adv. Mater. 29, 1606221.
Barea, E., Montoro, C., Navarro, J.A., 2014. Toxic gas removal–metal–organic frameworks for the capture and degradation of toxic gases and vapours. Chem. Soc. Rev. 43, 5419–5430.
Zhang, X., Zhang, G., Zhang, H., Liu, X., Shi, J., Shi, H., Yao, X., Chu, P.K., Zhang, X., 2020. A bifunctional hydrogel incorporated with CuS@ MoS2 microspheres for disinfection and improved wound healing. Chem. Eng. J. 382, 122849.
Chou, T.-M., Chan, S.-W., Lin, Y.-J., Yang, P.-K., Liu, C.-C., Lin, Y.-J., Wu, J.-M., Lee, J.-T., Lin, Z.-H., 2019. A highly efficient Au-MoS2 nanocatalyst for tunable piezocatalytic and photocatalytic water disinfection. Nano Energy 57, 14–21.
Meng, X., Li, Z., Zeng, H., Chen, J., Zhang, Z., 2017. MoS2 quantum dots-interspersed Bi2WO6 heterostructures for visible light-induced detoxification and disinfection. Appl. Catal. B: Environ. 210, 160–172.
Liu, C., Kong, D., Hsu, P.-C., Yuan, H., Lee, H.-W., Liu, Y., Wang, H., Wang, S., Yan, K., Lin, D., 2016. Rapid water disinfection using vertically aligned MoS 2 nanofilms and visible light. Nat. Nanotechnol. 11, 1098–1104.
Vilela, D., Stanton, M.M., Parmar, J., Sánchez, S., 2017. Microbots decorated with silver nanoparticles kill bacteria in aqueous media. ACS Appl. Mater. Interfaces 9, 22093–22100.
Park, J., Du, P., Jeon, J.K., Jang, G.H., Hwang, M.P., Han, H.S., Park, K., Lee, K.H., Lee, J. W., Jeon, H., 2015. Magnesium corrosion triggered spontaneous generation of H2O2 on oxidized titanium for promoting angiogenesis. Angew. Chem. Int. Ed. 54, 14753–14757.
Park, S.Y., Jung, Y.W., Hwang, S.H., Jang, G.H., Seo, H., Kim, Y.-C., Ok, M.-R., 2018. , Instrument-free and autonomous generation of H2O2 from Mg–ZnO/Au hybrids for disinfection and organic pollutant degradations. Met. Mater. Int. 24, 657–663.
Kaila, V.R., Wikström, M., 2021. Architecture of bacterial respiratory chains. Nat. Rev. Microbiol. 19, 319–330.
Volentini, S.I., Farías, R.N., Rodríguez-Montelongo, L., Rapisarda, V.A., 2011. Cu (II)-reduction by Escherichia coli cells is dependent on respiratory chain components. Biometals 24, 827–835.
Rensing, C., Grass, G., 2003. Escherichia coli mechanisms of copper homeostasis in a changing environment. FEMS Microbiol. Rev. 27, 197–213.
Wang, G., Feng, H., Gao, A., Hao, Q., Jin, W., Peng, X., Li, W., Wu, G., Chu, P.K., 2016. Extracellular electron transfer from aerobic bacteria to Au-loaded TiO2 semiconductor without light: a new bacteria-killing mechanism other than localized surface plasmon resonance or microbial fuel cells. ACS Appl. Mater. Interfaces 8, 24509–24516.
Mei, L., Teng, Z., Zhu, G., Liu, Y., Zhang, F., Zhang, J., Li, Y., Guan, Y., Luo, Y., Chen, X., 2017. Silver nanocluster-embedded zein films as antimicrobial coating materials for food packaging. ACS Appl. Mater. Interfaces 9, 35297–35304.
Sharma, V.K., Yngard, R.A., Lin, Y., 2009. Silver nanoparticles: green synthesis and their antimicrobial activities. Adv. Colloid Interface Sci. 145, 83–96.
Carlson, C., Hussain, S.M., Schrand, A.M., Braydich-Stolle, L.K., Hess, K.L., Jones, R.L., Schlager, J.J., 2008. Unique cellular interaction of silver nanoparticles: size-dependent generation of reactive oxygen species. J. Phys. Chem. B 112, 13608–13619.

Møller, P., Hilbert, L.R., Corfitzen, C.B., Albrechtsen, H.-J., 2007. A new approach for biologically inhibiting surfaces. J. Appl. Surf. Finish. 2, 149–157.
Ge, Y., Liu, J., Jiang, T., Hao, Y., Shen, X., Gong, Z., Qi, Z., Yao, J., 2022. Self-disinfecting carbon filter: in situ spontaneous generation of reactive oxidative species via oxygen reduction reaction for efficient water treatment. Colloids Surf. A: Physicochem. Eng. Asp., 129266
Pizzutilo, E., Kasian, O., Choi, C.H., Cherevko, S., Hutchings, G.J., Mayrhofer, K.J., Freakley, S.J., 2017. Electrocatalytic synthesis of hydrogen peroxide on Au-Pd nanoparticles: from fundamentals to continuous production. Chem. Phys. Lett. 683, 436–442.
Siahrostami, S., Verdaguer-Casadevall, A., Karamad, M., Deiana, D., Malacrida, P., Wickman, B., Escudero-Escribano, M., Paoli, E.A., Frydendal, R., Hansen, T.W., 2013. Enabling direct H 2 O 2 production through rational electrocatalyst design. Nat. Mater. 12, 1137–1143.
Erdmann, M., Kleinbub, S., Wachtendorf, V., Schutter, J.D., Niebergall, U., Böhning, M., Koerdt, A., 2020. Photo-oxidation of PE-HD affecting polymer/fuel interaction and bacterial attachment. npj Mater. Degrad. 4, 18.
D.J. Stewart, The sulphate-reducing bacteria, 2nd ed, Endeavour, 8 (1984).
Paulus, U.A., Schmidt, T.J., Gasteiger, H.A., Behm, R.J., 2001. Oxygen reduction on a high-surface area Pt/Vulcan carbon catalyst: a thin-film rotating ring-disk electrode study. J. Electroanal. Chem. 495, 134–145.
Jiang, Y., Ni, P., Chen, C., Lu, Y., Yang, P., Kong, B., Fisher, A., Wang, X., 2018. Selective electrochemical H2O2 production through two-electron oxygen electrochemistry. Adv. Energy Mater. 8, 1801909.
Nosaka, Y., Nosaka, A.Y., 2017. Generation and Detection of Reactive Oxygen Species in Photocatalysis. Chem. Rev. 117, 11302–11336.
Ferreira, L., Guedes, J.F., Almeida-Aguiar, C., Fonseca, A.M., Neves, I.C., 2016. Microbial growth inhibition caused by Zn/Ag-Y zeolite materials with different amounts of silver. Colloids Surf. B: Biointerfaces 142, 141–147.
Ferreira, L., Almeida-Aguiar, C., Parpot, P., Fonseca, A.M., Neves, I.C., 2015. Preparation and assessment of antimicrobial properties of bimetallic materials based on NaY zeolite. RSC Adv. 5, 37188–37195.
Jiao, L., Lin, F., Cao, S., Wang, C., Wu, H., Shu, M., Hu, C., 2017. Preparation, characterization, antimicrobial and cytotoxicity studies of copper/zinc-loaded montmorillonite. J. Anim. Sci. Biotechnol. 8, 1–7.
Bakina, O., Glazkova, E., Svarovskaya, N., Rodkevich, N., Lerner, M., 2019. "Janus"-like Cu-Fe bimetallic nanoparticles with high antibacterial activity. Mater. Lett. 242, 187–190.
Andrade, G.R., Nascimento, C.C., Lima, Z.M., Teixeira-Neto, E., Costa, L.P., Gimenez, I.F., 2017. Star-shaped ZnO/Ag hybrid nanostructures for enhanced photocatalysis and antibacterial activity. Appl. Surf. Sci. 399, 573–582.
Cai, S., Jia, X., Han, Q., Yan, X., Yang, R., Wang, C., 2017. Porous Pt/Ag nanoparticles with excellent multifunctional enzyme mimic activities and antibacterial effects. Nano Res. 10, 2056–2069.
Guridi, A., Diederich, A.-K., Aguila-Arcos, S., Garcia-Moreno, M., Blasi, R., Broszat, M., Schmieder, W., Clauss-Lendzian, E., Sakinc-Gueler, T., Andrade, R., 2015. New antimicrobial contact catalyst killing antibiotic resistant clinical and waterborne pathogens. Mater. Sci. Eng.: C. 50, 1–11.
Wang, G., Tang, K., Meng, Z., Liu, P., Mo, S., Mehrjou, B., Wang, H., Liu, X., Wu, Z., Chu, P.K., 2020. A quantitative bacteria monitoring and killing platform based on electron transfer from bacteria to a semiconductor. Adv. Mater. 32, 2003616.
Chen, J., Qin, Z., Martino, T., Shoesmith, D., 2017b. Non-uniform film growth and micro/macro-galvanic corrosion of copper in aqueous sulphide solutions containing chloride. Corros. Sci. 114, 72–78.
Berrocal, C.G., Lundgren, K., Löfgren, I., 2016. Corrosion of steel bars embedded in fibre reinforced concrete under chloride attack: state of the art. Cem. Concr. Res. 80, 69–85.
Ni, Q., Xia, X., Zhang, J., Dai, N., Fan, Y., 2017. Electrochemical and SVET studies on the typical polarity reversal of Cu–304 stainless steel galvanic couple in Cl−-containing solution with different pH. Electrochim. Acta 247, 207–215.